Available online at www.sciencedirect.com
SCIENCE DIRECT®
Icarus 180 (2006) 201–216
ICARUS
www.elsevier.com/locate/icarus

Binary near-Earth asteroid formation: Rubble pile model of tidal disruptions

Kevin J. Walsh *, Derek C. Richardson

Department of Astronomy, University of Maryland, College Park, MD 20740-2421, USA

Received 20 April 2005; revised 28 July 2005

Available online 27 October 2005

Abstract

We present numerical simulations of near-Earth asteroid (NEA) tidal disruption resulting in bound, mutually orbiting systems. Using a rubble pile model we have constrained the relative likelihoods for possible physical and dynamical properties of the binaries created. Overall 110,500 simulations were run, with each body consisting of ∼1000 particles. The encounter parameters of close approach distance and velocity were varied, as were the bodies' spin, elongation and spin axis direction. The binary production rate increases for closer encounters, at lower speeds, for more elongated bodies, and for bodies with greater spin. The semimajor axes for resultant binaries are peaked between 5 to 20 primary radii, and there is an overall trend for high eccentricity, with 97% of binaries having $e > 0.1$. The secondary-to-primary size ratios of the simulated binaries are peaked between 0.1 and 0.2, similar to trends among observed asteroid binaries. The spin rates of the primary bodies are narrowly distributed between 3.5- and 6-h periods, whereas the secondaries' periods are more evenly distributed and can exceed 15-h periods. The spin axes of the primary bodies are very closely aligned with the angular momenta of the binary orbits, whereas the secondary spin axes are nearly random. The shapes of the primaries show a large distribution of axis ratios, where those with low elongation (ratio of long and short axis) are both oblate and prolate, and nearly all with large elongation are prolate. This work presents results that suggest tidal disruption of gravitational aggregates can make binaries physically similar to those currently observed in the NEA population. As well, tidal disruption may create an equal number of binaries with qualities different from those observed, mostly binaries with large separation and with elongated primaries.

Keywords: Asteroids; Dynamics; Rotational dynamics; Tides, solid body

1. Introduction

1.1. Motivation

The discovery and observation of binary asteroids over the past decade have provided new ways to study the properties of Solar System bodies. Before the 1993 Galileo mission discovery of Ida's companion Dactyl in the main asteroid belt, there were unconfirmed detections and theoretical speculation about binary asteroids. van Flandern et al. (1979) reported on anomalous occultations of Main Belt Asteroids (MBAs) (6) Hebe, (532) Herculina, and (18) Melpomene, which suggested the existence of companions, but these observations have never been confirmed.

Cellino et al. (1985) published anomalous lightcurves for 10 objects, one of which has since been shown to be a contact binary, (216) Kleopatra (Ostro et al., 2000a; Merline et al., 2000a; Tanga et al., 2001). Gehrels et al. (1987) and Gradie and Flynn (1988) searched MBAs via imaging and coronagraphic techniques, neither detecting any binaries. After the discovery of Dactyl, Roberts et al. (1995) examined 57 asteroids with speckle interferometry, failing to discover any companions. Pravec and Hahn (1997) used lightcurve measurements to make a very strong case for a companion to NEA 1994 AW_1, by observing a lightcurve with two components and occultations/eclipses. Similarly, NEAs 1991 VH, 3671 Dionysus and 1996 FG_3 were considered highly probable targets using similar methods (Mottola and Lahulla, 2000; Pravec et al., 2000b, 2005). Storrs et al. (1999) inspected 10 with HST and found no binaries.

Merline et al. (1999a) were the first to definitively find a companion with Earth-based methods by direct imaging of (45) Eugenia. Radar observations in 1999 demonstrated the exis-

* Corresponding author. Fax: +1 301 314 9067.
E-mail address: kwalsh@astro.umd.edu (K.J. Walsh).

0019-1035/$ – see front matter
doi:10.1016/j.icarus.2005.08.015

tence of NEA binaries 2000 DP_{107} and 2000 UG_{11} (Ostro et al., 2000b; Margot et al., 2002; Nolan et al., 2000). Since then, 24 NEA binaries have been found using lightcurves and radar observations. Binaries have also been observed in the Main Belt, Kuiper Belt and the Trojan population.

Bottke and Melosh (1996a, 1996b), citing the frequency of occurrence of doublet craters on terrestrial planets, investigated the effects of planetary flybys on contact binaries. This effort estimated that ∼15% of Earth-crossing asteroids could be binaries. Richardson et al. (1998) used N-body simulations of "rubble pile" asteroids disrupting during close encounters with Earth and also estimated that ∼15% of NEAs could be binaries. These N-body simulations were very similar to the ones presented in this current paper.

Tidal disruption has been credited with a large role in binary formation among NEAs due to some of the prominent similar properties shared by these binaries (Merline et al., 2002c; Margot et al., 2002). Understanding how tidal disruption creates binary asteroids is thus extremely important because this formation mechanism can shed light on the interior structure of NEAs, elucidate the history and evolution of NEAs, and may aid in future discovery of NEA binaries.

Studies suggest tidal disruption can also change the shape of bodies, make crater chains and doublet craters, and create or tear apart binaries (Solem and Hills, 1996; Schenk et al., 1996; Bottke et al., 1997, 1999; Richardson et al., 1998; Merline et al., 2002c). Here we study in detail the properties of the NEA binaries created by numerical simulations of tidal disruption.

1.1.1. Observed NEA binaries

The known NEA binaries have been discovered from a combination of lightcurve and radar observations. Lightcurve studies have been conducted on a large number of bodies, but certain orbital properties (asynchronous orbit and favorable geometry) are needed to make an unambiguous assessment of the state of the binary (Weidenschilling et al., 1989; Pravec and Hahn, 1997). The secondaries must be large enough (∼20% of the primary) for their nonsynchronous periods to be observed above any noise in the lightcurve of the primaries. Observations must also capture multiple occultations/eclipses over multiple revolutions of the secondary body, which requires extensive observations at a viewing angle near the binary orbital plane.

Radar observations require the close approach of an asteroid to Earth, but can provide detailed physical and orbital information about the binary. The signal-to-noise ratio (SNR) of radar measurements is proportional to $R_{\rm tar}^{-4}$ and $D_{\rm tar}^{3/2}$, where $R_{\rm tar}$ and $D_{\rm tar}$ are the distance to and diameter of the target body, respectively. The SNR is also proportional to $P^{1/2}$, the square root of the rotation period. Thus radar observations are more likely to discover nearby, larger, slower rotating secondaries (Ostro et al., 2002).

The currently known NEA binaries share similar physical and orbital traits. All currently known or suspected binaries have primary bodies with a diameter ($D_{\rm pri}$) less than 4 km (see Table 1). All primaries with measured rotations, with the exceptions of NEAs 69230 Hermes and 2000 UG_{11}, have rotation periods between 2.2 and 3.6 h. The critical spin limit for a spherical strengthless body is approximately given by

$$P_{\rm crit} \approx \frac{3.3}{\sqrt{\rho}}\ \text{(h)}, \tag{1}$$

where ρ, the bulk density of the body, is in g cm^{-3}. For a body with $\rho = 2.2$ g cm^{-3}, $P_{\rm crit} \approx 2.2$ h, which defines the lower limit for primary spin rate (Pravec and Harris, 2000).

All the primaries have similar lightcurve amplitudes, typically below 0.2 mag. The amplitude of a primary's lightcurve (Δm) has a simple relationship with the bodies shape

$$\Delta m \sim 2.5 \log \frac{a}{b}, \tag{2}$$

where a and b are the long and intermediate length axes of a triaxial ellipsoid. Thus the largest lightcurve amplitudes observed, ∼0.2 mag, imply a 1.2:1.0 axis ratio. The entire population of NEAs has a much larger range of lightcurve amplitudes; 0.2 is relatively close to spherical in comparison (Pravec and Harris, 2000).

The secondaries have diameters typically between 0.2 and 0.6 times the diameter of the primary ($D_{\rm pri}$). Again, the exception is Hermes which is a suspected synchronously rotating binary with equal-sized components. All others are asynchronous systems, with the primary rotating much faster than the orbital period of the secondary (Pravec et al., 2004b). An observational limit exists for bodies below 0.2 $D_{\rm pri}$, but between 0.6 and 1.0 $D_{\rm pri}$, no biases are known. The secondaries are also consistent in their separation from the primary, with most being within 6 primary radii ($R_{\rm pri}$). The exception is 1998 ST_{27} with a separation ∼10 $R_{\rm pri}$, which also has a relatively fast-spinning secondary (period <6 h) and a high eccentricity ($e > 0.3$). Other than ST_{27}, the few eccentricities that are known are all below 0.1. Few rotations of secondaries are well known, though they appear mostly synchronized with the orbital motion, with 1998 ST_{27} again being an exception (Pravec et al., 2004b).

1.1.2. Main Belt asteroid binaries vs near-Earth asteroid binaries

Binaries in the Main Belt population (roughly in orbits with 2–4 AU semimajor axis) share few similarities with the NEAs just discussed. First, Main Belt asteroid binaries have been observed to have a much smaller percentage of occurrence (∼2–3%) than NEA binaries (∼15%) (Pravec et al., 1999; Margot et al., 2002; Merline et al., 2002c). Even accounting for different discovery techniques and observing scenarios there is a significant, sizable difference in relative numbers. Second, all but a few have primaries that are larger than 4.5 km, with nearly half larger than 100 km. Thus nearly all the primaries for known MBA binaries are larger than the largest NEA (4 km). Third, the primaries' spin periods are spread between 2.6 and 16.5 h, with only three with periods below 4.0 h (see Fig. 1, Table 2). This differs significantly from the very tight grouping of primary spin for NEAs. Fourth, the secondaries are between 0.04 and 1.0 times the size of the primaries, going well below the 0.2 size threshold for NEA binaries (the 0.2 size threshold is likely an observational bias for NEAs, rather than a physical limit).

Table 1
Orbital and physical properties for well-observed or suspected NEA binaries

Binary	a (AU)	e	D_{pri} (km)	P_{pri} (h)	a (km)	D_{sec} (km)	P_{orb} (d)	Discovery	References
(66391) 1999 KW_4	0.64	0.68	1.2	2.77	2.5	0.4	0.73	R	[1,2]
1998 ST_{27}	0.81	0.53	0.8	3.0	4.0	0.12		R	[3,4]
1999 HF_1	0.81	0.46	3.5	2.32	7.0	0.8	0.58	L	[2,5]
(5381) Sekhmet	0.94	0.29	1.0	2.7	1.5	0.3	0.52	R	[6,7]
(66063) 1998 RO_1	0.99	0.72	0.8	2.49	1.4	0.38	0.60	L	[2,8]
1996 FG_3	1.05	0.35	1.5	3.59	2.6	0.47	0.67	L	[2,9,10]
(88710) 2001 SL_9	1.06	0.27	0.8	2.40	1.4	0.22	0.68	L	[2,11]
1994 AW_1	1.10	0.07	1.0	2.52	2.3	0.5	0.93	L	[2,12]
2003 YT_1	1.10	0.29	1.0	2.34	2.7	0.18	1.25	L/R	[2,13]
(35107) 1991 VH	1.13	0.14	1.2	2.62	3.2	0.44	1.36	L	[2,14]
2000 DP_{107}	1.36	0.37	0.8	2.77	2.6	0.3	1.76	R	[2,15,16,17]
(65803) Didymos	1.64	0.38	0.8	2.26	1.1	0.17	0.49	L/R	[2,18]
(69230) Hermes	1.65	0.62	0.6	13.89			0.54	R	[2,19]
1990 OS	1.67	0.46	0.3		0.6	0.05	0.88	R	[20]
(5407) 1992 AX	1.83	0.27	3.9	2.55	6.8	0.78	0.56	L	[2,21]
2002 BM_{26}	1.83	0.44	0.6	2.7		0.1		R	[22]
(85938) 1999 DJ_4	1.85	0.48	0.4	2.51	0.8	0.17	0.74	L	[2,23,24]
2000 UG_{11}	1.92	0.57	0.2	4.44	0.4	0.08	0.77	R	[2,25]
2003 SS_{84}	1.93	0.57	0.1			0.06		R	[26]
2002 KK_8	1.95	0.46	0.5			0.1		R	[27]
(31345) 1998 PG	2.01	0.39	0.9	2.52	1.5	0.3		L	[2,28]
(3671) Dionysus	2.19	0.54	1.5	2.71	3.8	0.3	1.16	L	[2,29]
2002 CE_{26}	2.23	0.55	3.0	3.29	5.1	0.21	0.67	R	[2,30]
2005 AB	3.21	0.65		3.33			0.75	L	[31]

The discovery techniques are (L) lightcurve and (R) radar. References: [1] Benner et al. (2001b); [2] Pravec et al. (2005); [3] Benner et al. (2001a); [4] Benner et al. (2003); [5] Pravec et al. (2002); [6] Nolan et al. (2003b); [7] Neish et al. (2003); [8] Pravecn et al. (2003b); [9] Pravec et al. (2000b); [10] Mottola and Lahulla (2000); [11] Pravec et al. (2001); [12] Pravec and Hahn (1997); [13] Nolan et al. (2004); [14] Pravec et al. (1998); [15] Ostro et al. (2000b); [16] Pravec et al. (2000a); [17] Margot et al. (2002); [18] Pravec et al. (2003a); [19] Margot et al. (2003); [20] Ostro et al. (2003); [21] Pravec et al. (2000b); [22] Nolan et al. (2002a); [23] Pravec et al. (2004a); [24] Benner et al. (2004); [25] Nolan et al. (2000); [26] Nolan et al. (2003a); [27] Nolan et al. (2002b); [28] Pravec et al. (2000b); [29] Mottola et al. (1997); [30] Shepard et al. (2004); [31] Reddy et al. (2005).

Fifth, the observed separations are quite large, ranging from 2 to 100 primary radii, well beyond any observed for NEAs.

The different discovery techniques and different formation mechanisms of MBA binaries are likely the cause of many of stark differences in the two groups. Most MBA binaries are discovered via adaptive optics (AO) observations, which preferentially find distant companions, outside of the point spread function of the brighter primary. These observations are also sensitive to large brightness differences, for example (45) Eugenia's moon Petit Prince was 7 mag dimmer at discovery than its primary (Merline et al., 2002c). These two effects demand that the observed MBA binaries have large separations and allow a wide range of size ratios.

Another limiting factor is primary size. This is a complication regardless of observing technique, as a 1-km body in the Main Belt is substantially more difficult to study than one in the near-Earth population.

Primary spin rate is a quantity which should not be biased in AO observations. The differences in primary spin between MBA and NEA binaries is commonly cited as the main evidence for different formation scenarios. With well-correlated primary spins, NEA binaries likely result from some kind of spin-up mechanism acting on the primary, with disruption and capture happening after the asteroid spins past its breakup limit.

Currently it may be safe to consider a typical NEA binary (with a primary diameter of ∼1 km and a small, close

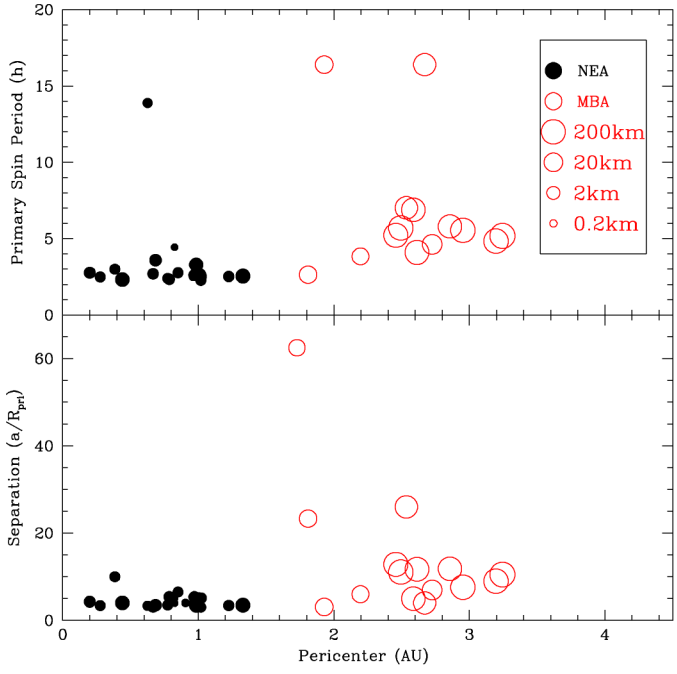

Fig. 1. (Top) The primary rotation period of the known NEA (filled) and MBA (open) binaries as a function of the pericenter of the binary's orbit. (Bottom) The component separations of the same binaries as a function of pericenter. In both panels, each point represents one binary, with the size of the point proportional the size of the primary.

Table 2
Orbital and physical properties for well-observed or suspected MBA binaries

Binary	a (AU)	e	D_{pri} (km)	P_{pri} (h)	a (km)	D_{sec} (km)	P_{orb} (d)	Discovery	References
(4674) Pauling	1.86	0.07	8		250	2.5		AO	[1]
(1509) Esclangona	1.87	0.03	12	2.64	140	4		AO	[2,3]
(9069) Hovland	1.91	0.11	3	4.22		0.9		L	[4]
(5905) Johnson	1.91	0.07	5.0	3.783		2.0	0.91	L	[4,5]
(1089) Tama	2.21	0.13	13	16.44	20	(9)	0.68	L	[6]
(3749) Balam	2.24	0.11	7		350	1.5	100	AO	[7,8]
(854) Frostia	2.36	0.17					1.57	L	[9]
(3782) Celle	2.41	0.09	6.1	3.84	20.0	2.6	1.52	L	[10,11]
(1313) Berna	2.65	0.20		25.464			1.061	L	[12]
(45) Eugenia	2.72	0.08	215	5.70	1190	13	4.69	AO	[8,13]
(4492) Debussy	2.76	0.17		26.59			1.11	L	[14]
(22899) 1999 TO_{14}	2.84	0.08	4.5		170	1.5		HST	[15]
(17246) 2000 GL_{74}	2.84	0.02	4.5		230	2		HST	[16]
(243) Ida	2.86	0.05	31	4.63	108	1.4	1.54	SC	[8,17]
(22) Kalliope	2.91	0.10	181	4.14	1020	38	3.58	AO	[18,19,20]
(283) Emma	3.04	0.15	148	6.88	600	12	3.36	AO	[21,22,23]
(130) Elektra	3.12	0.21	182	5.22	1250	4	3.9	AO	[21,24,25]
(379) Huenna	3.13	0.19	92	7.02	3400	(7)	81	AO	[23,26,27]
(90) Antiope	3.16	0.16	85	16.50	170	85	0.69	AO	[8,28]
(762) Pulcova	3.16	0.09	137	5.84	810	20	4.0	AO	[8,29]
(121) Hermione	3.43	0.14	209	5.55	775	13	2.57	AO	[30,31,32,33]
(107) Camilla	3.47	0.08	223	4.84	1240	9	3.71	HST	[8,34]
(87) Sylvia	3.49	0.07	261	5.18	1370	15	3.66	AO	[8,35]

The discovery techniques are (L) lightcurve, (AO) adaptive optics, (T) ground-based telescope, (SC) for spacecraft, and (HST) for Hubble space telescope. References: [1] Merline et al. (2004); [2] Merline et al. (2003b); [3] Warner (2004); [4] Warner et al. (2005a); [5] Warner et al. (2005b); [6] Behrend et al. (2004b); [7] Merline et al. (2002a); [8] Merline et al. (2002c); [9] Behrend et al. (2004a); [10] Ryan et al. (2003); [11] Ryan et al. (2004); [12] Behrend (2004c); [13] Merline (1999b); [14] Behrend (2004); [15] Merline et al. (2003d); [16] Tamblyn et al. (2004); [17] Belton and Carlson (1994); [18] Merline et al. (2001); [19] Margot et al. (2001); [20] Marchis et al. (2003); [21] Marchis et al. (2005); [22] Merline (2003c); [23] Stanzel (1978); [24] Merline et al. (2003e); [25] Magnusson (1990); [26] Margot and Keck (2003); [27] Harris et al. (1992); [28] Merline et al. (2000b); [29] Merline et al. (2000a); [30] Merline et al. (2002b); [31] Merline et al. (2003a); [32] Marchis et al. (2004a); [33] Marchis et al. (2004b); [34] Storrs et al. (2001); [35] Brown et al. (2001).

secondary) to be extremely difficult to observe in the Main Belt. Adaptive optics would have trouble detecting secondaries with small separations, whereas high precision lightcurves require a long baseline of observations on reasonably large telescopes. Recent discoveries in the Main Belt have started pushing the small end of the MBA binary size boundaries, with two lightcurve discoveries of binaries with D_p below 5 km, and AO discoveries with D_p below 10 km. However, the number of these small Main Belt binaries is not yet large enough to study their statistics in detail.

1.1.3. Tidal encounters and the origin of binaries

Tidal disruption of a rubble pile[1] has been invoked to explain the disruption of Comet D/Shoemaker–Levy 9 (SL9) and has also been applied to asteroid studies. SL9 disrupted when the comet passed within ∼1.36 R_J of Jupiter on 1992 July 7. The comet was torn apart and ∼21 fragments or reaccumulated clumps were later observed. N-body studies have since matched many of the comet's basic post-disruption features (train length, position angle, and morphology) using a strengthless rubble pile model (Solem, 1994; Asphaug and Benz, 1996; Walsh et al., 2003).

Solem and Hills (1996) used similar N-body techniques to simulate the change in elongation (ratio of long axis to short axis length) of an asteroid due to a planetary close approach. Citing 1620 Geographos as an extreme case with an elongation of 2.7, encounters with Earth between close approach distance $q = 1.02$ and 2.03 Earth radii ($R_\oplus$) were sampled with a range of v_∞ (the speed at infinity of a hyperbolic encounter) between ∼15 and 25 km s^{-1}. The models represented the progenitors with 135 particles, and some simulations produced outcomes more elongated than Geographos, providing a potential means of creating very elongated solar system bodies.

Bottke and Melosh (1996a) simulated splitting of contact binaries to explain doublet craters on Earth, Venus, and Mars. In this model a binary asteroid is formed during a close encounter with a planet, and the binary's separation grows through subsequent encounters. Eventually the binary hits a planet, making a doublet crater. This scenario depends on a constant refreshing of the NEA binary population via tidal disruptions, and predicts that ∼15% of NEAs may be binaries at any given time.

Simulations of NEA tidal disruption by Richardson et al. (1998) covered a large parameter space of elongated rotating bodies (constructed with 247 particles) passing Earth at various q and v_∞. The study was designed to quantify disruption and mass loss for tidal encounters, but noted binary formation as

[1] A rubble pile is a moderately porous, strengthless body with constituents bound only by their own self-gravity. See Richardson et al. (2002, 2005) for discussion of rubble piles, gravitational aggregates, and "perfect" numerical rubble piles.

an observed outcome and suggested that tidal disruption could explain up to ∼15% of the NEAs being binaries. The simulations sparsely covered the parameters of q, v_∞, progenitor elongation, progenitor spin rate and long axis alignment. Basic trends in disruption were observed, with increasing disruption for closer approaches, slower approach speeds, and faster prograde rotation rates. More subtle results were seen as a function of body elongation and long axis alignment at close approach.

Bottke et al. (1999) compared the shape of 1620 Geographos, obtained from delay-Doppler measurements, to that of a tidal encounter outcome. The well-defined shape of Geographos matched many features of the simulation output, including the cusped ends, an opposed convex side, and a nearly concave side with a large hump. This study was similar in approach to Solem and Hills (1996), but matched the high-quality images with high-resolution (∼500-particle) simulations.

Scheeres et al. (2000) provided analytical descriptions of rotation state changes to rigid bodies caused by close planetary flybys. This work has implications for the spin rate distribution of NEAs, which strongly influences binary creation. When this model was combined with a Monte Carlo sampling of planetary flybys, it demonstrated an overall increase in NEA spin rate, as well as a flyby-induced upper spin rate limit near 2 h (Scheeres et al., 2004).

Durda et al. (2004) simulated large-scale (100-km-diameter target body) catastrophic collisions of asteroids to determine the efficiency of forming binaries via collision. These simulations used a smoothed particle hydrodynamics (SPH) code to model the collision and an N-body code to simulate the post-collision evolution and reaccumulation of the fragments. The collisions were efficient at creating bound systems out of the reaccumulated debris and many of the binaries produced are qualitatively similar to those observed in the Main Belt. Michel et al. (2002, 2001) also noted binary formation in their SPH and N-body simulations of asteroid family formation.

The studies cited have investigated tidal disruption and distortion of NEAs using a rubble pile model and other techniques to simulate binary formation. The present study consists of a very large set of simulations designed to quantify many of the diagnostic qualities of binary NEAs created via tidal disruption. We adopt numerical techniques similar to those of previous N-body rubble pile simulations, and cover parameters previously shown to produce catastrophic tidal encounters, but in much greater detail. This study is unique in the large number of simulations performed and detailed investigation into the physical and orbital attributes of the resulting binaries. In Section 2 the details of the simulations and analysis are explained, and the results are discussed in Section 3. Conclusions and future work are presented in Section 4.

2. Method

2.1. Simulations

All simulations were done using `pkdgrav`, a parallelized tree code designed for efficient N-body gravitational and collisional simulations (Richardson et al., 2000, 2005; Leinhardt et al., 2000; Stadel, 2001; Leinhardt and Richardson, 2002). The simulations used a timestep of 10^{-5} yr$/2\pi$ (about 50 s, or ∼2% of the dynamical time for the particles) and all simulations were initially run for 10,000 timesteps (∼5.8 days). Simulations that produced binaries or systems of bound bodies were run an additional 20,000 timesteps to reach a total of 30,000 timesteps (∼17.4 days). The collisions of individual particles were governed by coefficients of restitution, both normal (ϵ_n) and tangential (ϵ_t), which determine how much energy is dissipated during collisions. The normal coefficient of restitution, ϵ_n, was fixed at 0.8 in these simulations, similar to previous studies, and ϵ_t was fixed at 1.0 (no surface friction). Previous work has shown that ϵ_n has little effect on the outcome of a tidal disruption so long as $\epsilon_n < 1.0$ (Richardson et al., 1998).

2.2. Progenitors

The rubble pile models used in these simulations consist of identical rigid spheres bound to one another by gravity alone. There were five separate progenitors used in the simulations, each with different elongations: 1.0, 1.25, 1.5, 1.75, and 2.0 (here elongation is defined as $e = a/c$ with a, b, and c representing the long, intermediate and short axis length of a tri-axial ellipsoid; in our simulations, b was set to $\sim c$). The bodies were all constructed using particles with an internal density of 3.4 g cm^{-3}, but the bulk density of the body would vary depending on its packing efficiency, which was usually around ∼60%, making a bulk density of ∼2.0 g cm^{-3}. Each progenitor consisted of approximately 1000 particles; the exact number varied between 991 and 1021 depending on the final overall shape.[2] Recent work by Richardson et al. (2005) shows that the resolution of a rubble pile simulation can have an effect on the outcome: as resolution increases, the granular behavior becomes more fluid-like, aiding disruption. To justify our use of 1000 particles, we assume the smallest building block for rubble piles in the inner Solar System is ∼150 m, based on SPH collision studies and the observed spin rate cutoff of kilometer-sized asteroids (Benz and Asphaug, 1999; Pravec et al., 2002). With 150-m particles, a spherical close-packed rubble pile with 1000 particles is ∼3.3 km in diameter. This diameter is nearly as large as the largest observed NEA binary primary, but also has enough resolution to model ejected fragments which may remain bound to each other, and to allow accurate measurement of size ratios.

The progenitors were given one of four rotation rates: 3-, 4-, 6-, or 12-h periods. Large asteroid ($D > 40$ km) spin rates have been shown to follow a Maxwellian distribution, but small asteroids ($D < 10$ km) have an excess of fast and slow rotators (Pravec et al., 2002). Studies have attempted to fit the popu-

[2] The packing algorithm uses hexagonal closest packing, which depends on a certain level of symmetry to construct bodies out of a finite number of perfect spheres. This results in variation in the number of particles for various shapes. Similarly, due to boundary algorithms and the finite size of the building blocks, the bulk density can vary slightly.

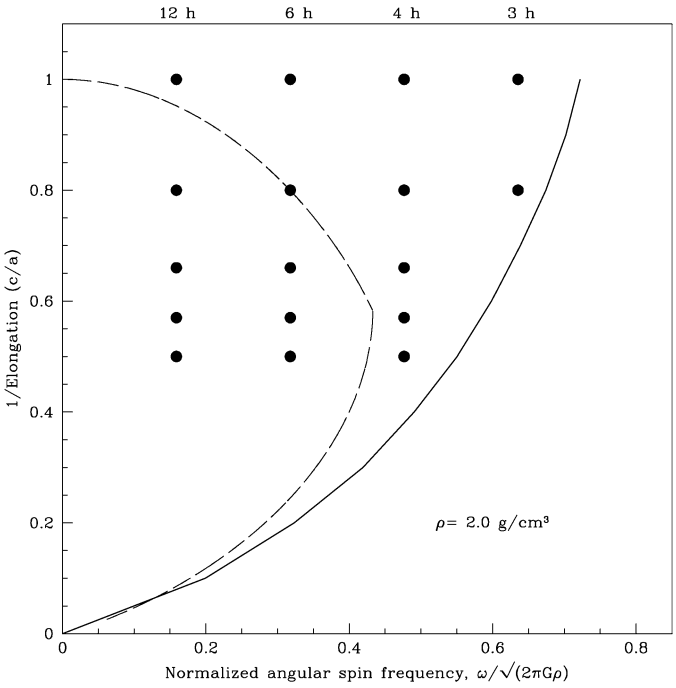

Fig. 2. Progenitor initial parameters of the reciprocal of elongation (c/a) and normalized angular spin frequency ($\omega/\sqrt{2\pi G\rho}$) are plotted as points. (solid line) This is compared with the limiting curve for a cohesionless granular proloid with friction angle $\phi = 40°$ (Holsapple, 2001; Richardson et al., 2005). (dashed line) The solutions for Jacobi and Maclaurin sequences representing theoretical axis ratios for rotating fluids.

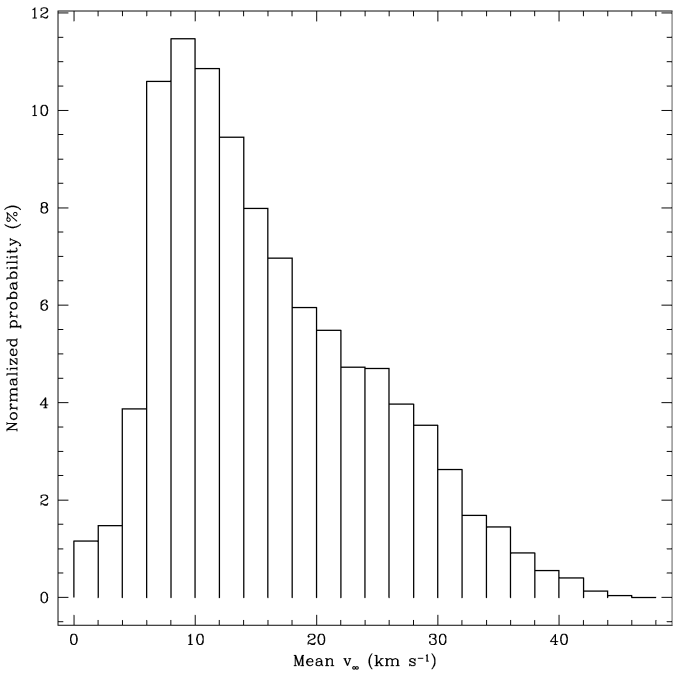

Fig. 3. The distribution of v_∞ for close hyperbolic encounters with Earth, with v_∞ in km s^{-1} and the y-axis indicating the normalized probability for each v_∞ bin (Bottke, personal communication, 2004).

lation of small asteroids with 3 different Maxwellians, with a combination of fast, moderate, and slow rotation rates of ∼6.4, 11.3, and 27.5 h (Donnison and Wiper, 1999). However, with the large proportion of fast-rotating NEAs (possibly as high as 50%) observed to be primaries of binary systems, they may have already experienced a tidal disruption and had their spin state altered (Margot et al., 2002; Scheeres et al., 2004). Our selections were made to sample fast rotators (3, 4 h), as well as some moderate ones (6, 12 h). No spin periods longer than 12 h were simulated due to the small contribution rotation actually makes to tidal disruption at slower spins (Richardson et al., 1998).

The 3-h spin rate simulations were only carried out for progenitors with an elongation of 1.0 and 1.25. Comparison to Richardson et al. (2005), as well as separate tests, indicate that bodies with elongation of 1.5 or greater would be unstable at a 3-h spin rate, thus shedding mass and distorting prior to encountering the tidal forces of Earth (Fig. 2). The subset of results for 3 h will be presented independent of the bulk of the studies.

The progenitors used in this work are all below the limit for cohesionless granular proloids with friction angle $\phi = 40°$ (Holsapple, 2001). This limit, verified by Richardson et al. (2005) as a rotational stability limit for numerical models of rubble piles, differs from the Maclaurin/Jacobi limits for fluid bodies (essentially a sequence of allowed equilibrium shapes). The Maclaurin/Jacobi sequence can be derived analytically and provides a useful fiducial for comparing less idealized models. For example, Guibout and Scheeres (2003) determined that when a body is spinning beyond the Jacobi limit, the flow of material on the surface of the body is towards the equator, whereas below the limit, the flow is towards the poles.

2.3. Tidal encounters/initial conditions

The hyperbolic encounters asteroids have with planets can be described by the close approach distance q and the relative speed at infinity v_∞. When $v_\infty \gg v_{esc}$ (where $v_{esc} = \sqrt{2GM/R}$), close approach is distributed with likelihood increasing as the square of the distance. This means that an asteroid is four times more likely to encounter Earth at 4 $R_\oplus$ than at 2 $R_\oplus$. The v_∞ of these encounters depends on the bodies' pre-encounter orbits. A distribution of expected encounter statistics was taken from a series of N-body simulations of NEA migration from major source regions in the Main Belt (3:1 mean-motion resonance with Jupiter, ν_6 secular resonance, Mars crossers; Bottke et al., 2002; Bottke, personal communication, 2004; the distribution is similar to the impact speed distribution of Bottke et al., 1994). This was used to determine the expected v_∞ for the hyperbolic encounters with Earth (Fig. 3). Simulated parameters were selected to cover the most frequently occurring encounters and those previously shown to create very disruptive encounters likely to form binaries, all sampled at a frequency to balance detail with computational expediency: $q = 1.2$, 1.4, 1.6, 1.8, 2.0, 2.2, 2.4, 2.6, 2.8, 3.0, 3.5, 4.0 and 4.5 $R_\oplus$ and $v_\infty = 8$, 12, 16, 20, and 24 km s^{-1}.

Richardson et al. (1998) determined that the orientation of a non-spherical body can have a significant effect on the outcome of a tidal disruption. Specifically when the leading long axis of a body is rotating towards or away the planet, disrup-

Fig. 4. Snapshots of a tidal disruption simulation that led to the formation of a binary asteroid. The frames span about 72 h.

Table 3
Cumulative statistics from all 110,500 simulations

Total binaries	T-PROS	T-EEBs	Prolate	Oblate	S-class	B-class	M-class
4939	4556	383	4692	246	226	2299	2414
			3-h spin periods; 1.0 and 1.25 elongations only				
798	702	96	740	58	59	357	382

Total binaries is simply a count of all systems observed in the simulations. T-PROS and T-EEBs represent the total binaries split into dynamical groups (see Section 3.2). Prolate and oblate columns separate the binaries according the shape of the primary body (see Section 3.1.3). The binaries are also separated according to the class of disruption in which they were formed, S-class being the most disruptive, followed by B-class and M-class (see Section 3.3).

tion is enhanced or suppressed, respectively. Near perigee the equipotential surface of the body is stretched in the direction of Earth, and particles may rearrange to fill that shape (see Fig. 4 for a representative disruption). So if the long axis is rotating away from the planet, the rotation of the body opposes the movement of the particles. Instead of parameterizing the specifics of body axis alignment, a compromise was made: for each set of encounter (q and v_∞) and body (elongation and spin rate) parameters, the simulation was run 100 times, each time randomizing the orientation of the body's spin axis. Thus, given that the hyperbolic encounters were always in the same plane, some bodies were spinning prograde and some retrograde with respect to the encounter with Earth, depending on the randomization outcome. The long axis position at perigee was also random. This means that each set of parameters has a distribution of possible outcomes rather than one unique solution.

2.4. Analysis

Identification of orbiting systems was done using the `companion` code (Leinhardt and Richardson, 2005). This code is optimized for extremely fast searches over all simulations, identifying and analyzing those with bound systems. First, each simulation was searched for re-accumulated clumps of particles (Leinhardt et al., 2000). Once the clumps were identified, those consisting of more than three particles were fed into `companion` to search for systems. Any bound clumps were then analyzed to obtain important physical parameters, such as spin vector, elongation, mass, radius and position/velocity vectors.

The code `companion` sorts binaries according to identification of the primary and secondary clumps. In a situation where a specific clump has multiple secondaries, it will be listed once for each. Thus a triple, or larger, system may result in the same primary being counted multiple times in the statistics presented. The situation of an hierarchical system, where a secondary body itself has an orbiting clump, will result in that body being counted as both a secondary and a primary.

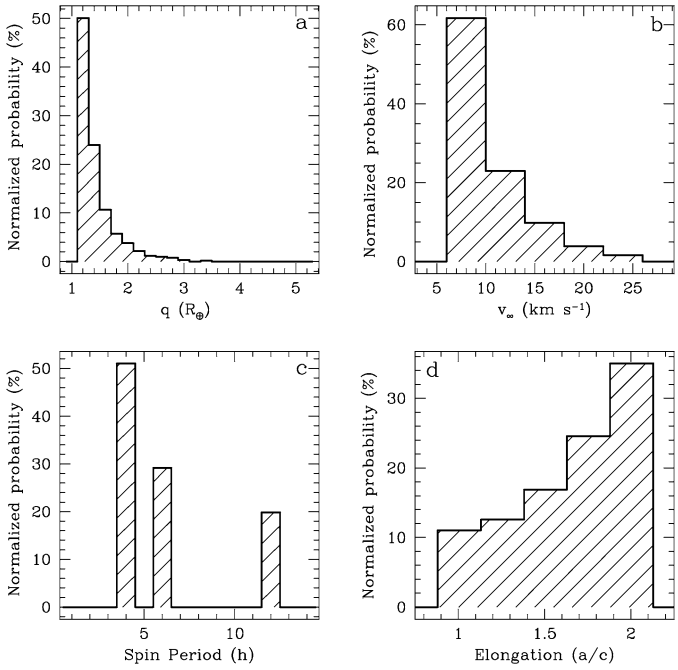

Fig. 5. Normalized probability of binaries formed versus (a) q, (b) v_∞, (c) initial spin rate, and (d) initial elongation.

3. Results and discussion

3.1. Bulk results

The bulk results covered 1105 sets of parameters, which encompasses 110,500 total simulations. From these simulations a total of 5737 bound systems were found after 30,000 timesteps (see Table 3 for a summary of bulk statistics). Of all the binaries, 798 were formed in the subset of 3 h, low-elongation simulations (to be referred to as the 3-h subset, and not included

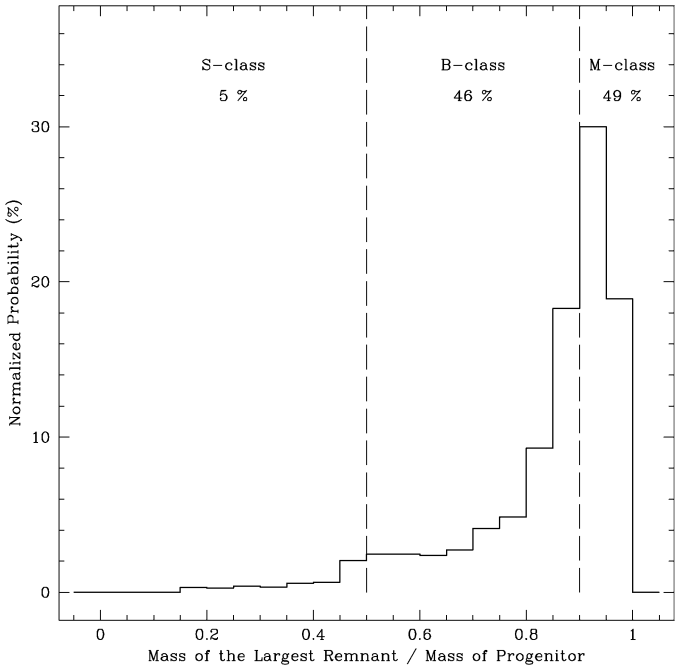

Fig. 6. Normalized probability of binaries formed versus the mass of the largest remnant divided by the mass of the progenitor. The vertical lines separate the disruptions into defined classes, with S-class being most disruptive, followed by B-class and M-class (Richardson et al., 1998). The percentages represent the total number of binaries in each class.

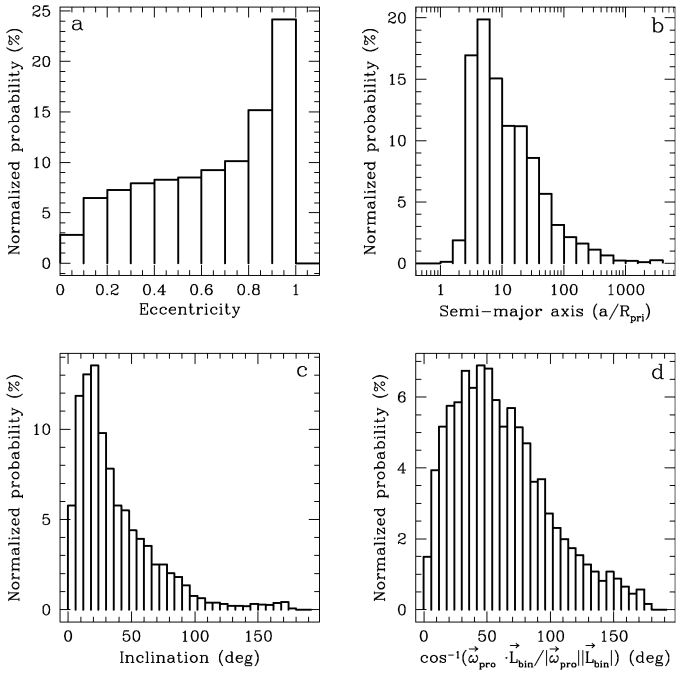

Fig. 7. (a) Satellite eccentricity and (b) semimajor axis (in terms of primary radii, $R_{\rm pri}$) distributions for binaries formed by tidal disruption. (c) Inclination of the orbit with respect to the encounter orbital plane, $i = \cos^{-1}((\mathbf{L}_{\rm bin} \cdot \mathbf{L}_{\rm enc})/(|\mathbf{L}_{\rm bin}||\mathbf{L}_{\rm enc}|))$. (d) Angle between the progenitor's spin axis, $\boldsymbol{\omega}_{\rm pro}$, and the binary angular momentum, $\mathbf{L}_{\rm bin}$.

in plots or tables unless specifically mentioned; see Sections 2.2 and 3.4).

Fig. 5 shows the relative contributions each parameter made to binary production. The trends are consistent with the findings of Richardson et al. (1998). The lower the v_∞, the more disruptive the outcome, and hence more binary formation results. Likewise binary production falls off very smoothly as q increases. The spin period distribution shows the dramatic increase in production at high spin rates, as bodies with 4-h periods were nearly 60% more likely to create a system than those with a 6-h period. Similarly, elongated bodies were significantly more efficient at producing binaries, with elongations of 2.0 making nearly 3 times the number of binaries as elongations of 1.0 or 1.25.

Fig. 6 displays the number of binaries formed as a function of the mass of the largest remnant divided by the mass of the progenitor, basically a measure of how disruptive the encounter was. This measure was used by (Richardson et al., 1998) to delineate 3 classes of tidally disruptive encounters:

1. S-class disruption: Named for an SL9-type disruption where the largest remnant has no more than 50% of the progenitor's mass. This class of disruptions is the most dramatic, as the progenitor is stretched into a long trail of particles before numerous clumps take shape. Binaries can be created if two clumps form close enough to become bound, or if a clump has accreted multiple fragments.
2. B-class disruption: A rotational breakup where the largest remnant contains between 50 and 90% of the mass of the progenitor. A B-class breakup involves a similar situation as the S-class, but less extreme, allowing a central large clump to form from the distorted and stretched progenitor.
3. M-class disruption: A mild breakup with less than 10% of the mass of the progenitor lost during the disruption. As the body is spun up, it is stretched along its long axis, particles slide to the equator of the body, and many are launched off the main body. Unlike the more disruptive breakups where a long chain of particles separates into separate clumps, the M-class encounters appear more like a body that starts spinning too fast (beyond the Jacobi and related cohesionless granular proloid limits), distorts, and then sheds mass from its equator.

Binary production peaks for encounters classified as M-class, with the largest remnant containing 90 to 95% of the mass of the progenitor. With a large percentage of the mass contained in the largest remnant, the binaries formed are limited to small size ratios. B-class and M-class outcomes account for nearly equal amounts of the binaries created and about 95% of the total created.

3.1.1. Orbital properties

The eccentricity distribution in the simulations is dominated by high ($e > 0.1$) eccentricities, and has similar morphology to the eccentricity distribution in Durda et al. (2004) found in binaries formed after MBA collisions (Fig. 7a). However, the known binary NEAs with measured eccentricity are usually found to have eccentricity below 0.1. Such systems are formed at one tenth the rate of those with $e > 0.9$ in our simulations and account for only ∼3% of the total results. This differ-

ence might be explained by lightcurve studies possibly being more likely to discover low-eccentricity secondaries or by evolutionary eccentricity damping (Weidenschilling et al., 1989; Murray and Dermott, 1999). Tidal dissipation mechanisms are expected to damp eccentricities, where the timescales are dependent on Q (the tidal dissipation parameter for the secondary), the diameter of the secondary, and the semimajor axis of the orbit (see Section 3.6).

The semimajor axis distribution is relatively smooth, peaked around 5 $R_{\rm pri}$ and extending out to nearly 1000 $R_{\rm pri}$ (Fig. 7b). The Hill sphere radius, $r_{\rm H} \sim a(M_{\rm pri}/3M_{\odot})^{1/3}$, where $M_{\odot}$ is the mass of the Sun, and $a = 1$ AU at Earth, equates to $r_{\rm H} \approx 130 R_{\rm pri}$. Thus inclusion of the Sun in these simulations would eventually eliminate many of the systems with very large separation, as Hamilton and Burns (1991) showed that circular prograde orbits are stable with respect to solar tides only out to $\sim r_{\rm H}/2$, and retrograde orbits are stable to $\sim r_{\rm H}$. The small number of binaries with $a < 2$ $R_{\rm pri}$ are expected to have extremely short lifetimes against collision with the primary (Scheeres, 2002). Observed NEA binaries nearly all have $a/R_{\rm pri}$ between 3 and 10, which is also the most likely outcome seen in the simulations. However, the simulations create many systems with larger separations that are not observed in the NEA population, suggesting a possible strong observational selection effect or an evolutionary/survival property. Nearly half the simulations produced a separation of over 10 $R_{\rm pri}$, which may suggest that we are only currently observing half of the NEA binaries.

The inclination of the binary favors an alignment with the progenitor's encounter orbit (0°), where inclination is measured as the angle between the plane of the encounter orbit and the plane of the binary orbit (see Fig. 7c). The inclination distribution peaks around 20°, and has some cases with values between 90° and 180°, which describe outcomes where the binary orbit is retrograde with respect to the progenitor's encounter with Earth. This could have come about if a progenitor had retrograde spin with respect to the encounter, or via a chance post-disruption circumstance, most likely involving a very small secondary.

The rest of the angular momentum of the system comes from the spin of the progenitor, which is quantified by measuring the angle between the spin axis of the progenitor and the binary's angular momentum vector ($\boldsymbol{\omega}_{\rm pro}$ and $\mathbf{L}_{\rm bin}$; see Fig. 7d). This has a peak around 45° falling off towards 0° and 90°, with very small contributions between 90° and 180°. This result suggests that neither progenitor spin nor encounter orbit will dominate the resultant binary inclination but that the encounter orbit is slightly more important. The encounter scenario likely determines which factor dominates, with a fast spinning progenitor disrupting at a distant q having the plane of the binary determined by the progenitor's spin, whereas a slow spinning, low q encounter placing debris mostly in the plane of the encounter.

3.1.2. Body properties

The size ratio between secondary and primary bodies is strongly peaked between 0.1 and 0.2 (Fig. 8a). This is a slightly lower and narrower peak than that observed for NEA binaries, for which size ratios typically range between 0.2 and 0.6, with the exception being Hermes, with a size ratio very near 1.0 (Margot et al., 2003; Pravec, 2003c). The lowest size ratios in the simulations were <0.05, which is limited by the arbitrary requirement we imposed that three particles are needed to make a clump, and various complications of measuring the elongated shapes of rubble piles. These two main disparities with observations, the width and position of the simulation size ratio peak, may potentially be an effect of the simulation resolution. If resolution affects resultant size ratios, and, as was discussed in Section 2.2, progenitors are constructed out of 150–200-m-diameter building blocks, then smaller progenitors would require lower resolution. This effect could potentially account for both the higher observed size ratios and their wide range, as a range in progenitor sizes might generate a wider peak in simulated size ratios. Another problem is potential irregular shapes and sizes of building blocks, which may differ significantly from the perfect hard spheres used for computation simplicity. On the other hand, lightcurve studies are limited by the size ratio, and cannot detect secondaries below 0.2 times the size of the primary (Merline et al., 2002c).

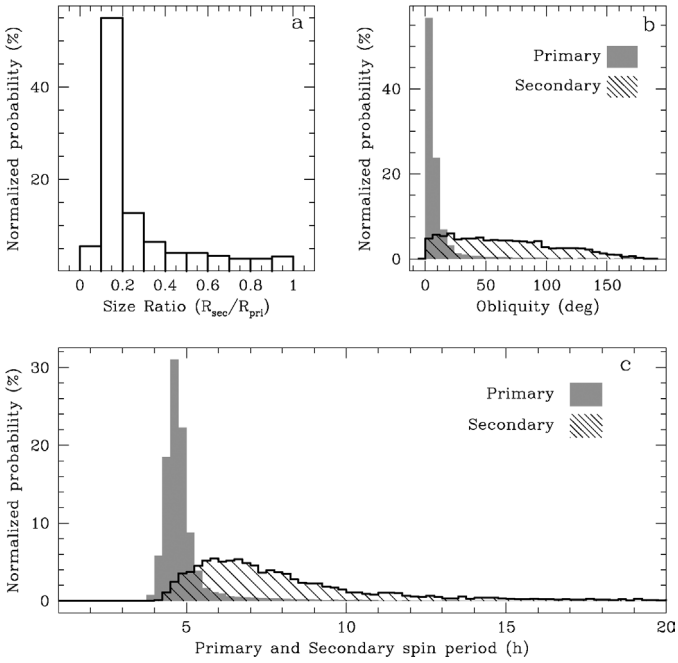

Fig. 8. (a) Normalized probability of binaries formed as a function of secondary-to-primary size ratio. (b) Primary (shaded) and secondary (cross-hatch) obliquity. (c) Primary (shaded) and secondary (cross-hatch) spin period.

The spin of the primary in the simulations is bracketed between 3.5- and 6.0-h spin periods, while the secondary has a peak around 6 h and falls off slowly out to 20 h and greater (Fig. 8c). The spin of the primary has been exceptionally consistent in observed NEA binaries, with nearly all measured to have spin periods between 2.2 and 3.6 h. This disparity between our simulations and the observations is potentially caused by our choice of parameters. The fastest progenitor spin period simulated was 3 h and likely does not represent the fastest spinning NEAs that encounter Earth. For the densities used in

the simulations, and following the work of Richardson et al. (2005), the critical spin period for a spherical rubble pile of the density we used is approximately 2.7 h (see Eq. (1)). This is significantly slower than the shortest observed periods in the NEA population; however, the observed distribution of spin rates for NEAs does not suggest that an overwhelming number have periods less than 3.0 h (Pravec et al., 2002). Some of the disparity may be the numerical simplifications needed for the simulations, notably perfect spherical particles, which could artificially inflate porosity and decrease critical spin rate. This could make the idealized rubble piles disrupt at a slower spin rate than observed. The bulk density of the progenitor is ∼2.0 g cm^{-3} with a porosity of 35%, neither of which are extreme for observed NEAs. However, any tensile forces or mechanical strength which could push critical spin rate faster, even very briefly, may contribute to the very fast spinning primary. Further work is needed to show whether these caveats are responsible for the difference between the observed and simulated spin rate distributions.

The obliquity of the primary in simulations is quite low (where obliquity is the angle between $\boldsymbol{\omega}_{\text{pri}}$ and $\mathbf{L}_{\text{bin}}$), with close to 90% of the binaries having an obliquity less than 20°. The obliquity of the secondary has no such relation, being nearly flat between 0° and 90°, and falling off from 90° to 180° (Fig. 8b). With many secondaries formed from accreting material in orbit around the primary, retaining an aligned spin axis appears to be unlikely for a secondary.

3.1.3. Shape of the primary

The shape of the primary was measured along the body's three principal axes, a, b, and c for the longest, intermediate and shortest axis length. Nearly all primaries are in a principal axis rotation state, rotating around the shortest axis. Thus the shape irregularities which are associated with a rotational lightcurve are a result of a difference between the long axis, a and the intermediate axis, b. If the intermediate axis, b, equals a or c, the body is either oblate ($b = a$) or prolate ($b = c$). However, few bodies approach such perfect classification, so for the sake of simplicity we define a shape index

$$I = (a - b)/(a - c),$$

where $I = 1$ means prolate, and $I = 0$ oblate.

The progenitor bodies were created to be simple prolate ellipsoids ($b = c$), with different values of a/c for varying amounts of elongation. The resulting primaries, as shown in Fig. 9a, have a distribution of a/c concentrated between 2.0 and 3.0. The progenitor elongations used in the simulation were only varied between 1.0 and 2.0, so elongation was significantly enhanced during the binary-forming encounters.

The distribution of a/b is a more valuable comparison to the shape derived via lightcurve studies for bodies rotating around their shortest principal axis. This distribution has the same peak as a/c, at 1.95, but a larger concentration of objects near 1.0 (Fig. 9b). When the distribution is separated into bodies with $I < 0.5$ and >0.5 (more oblate-like or prolate-like), the oblate-like bodies account for nearly half of these

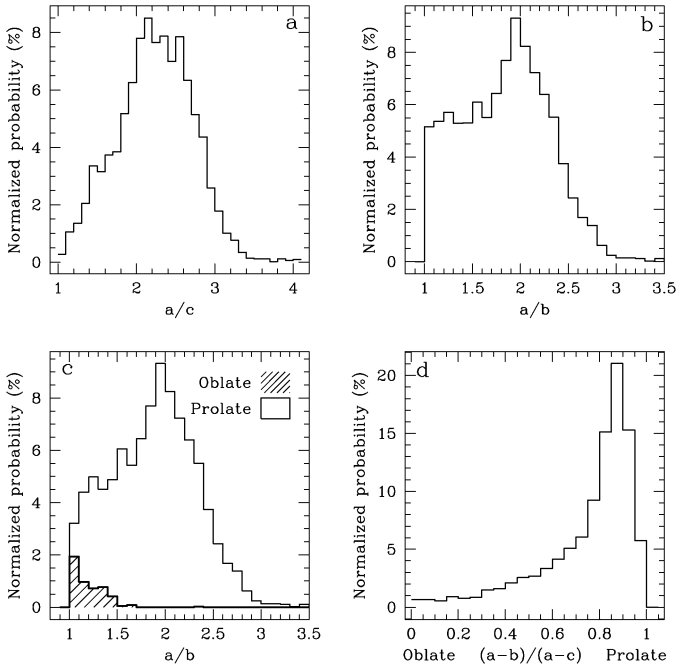

Fig. 9. (a) Ratio of axes a/c for primaries of resultant binary systems. (b) Ratio of axes a/b. (c) Ratio of axes a/b separated into prolate (thin lines) and oblate (thick lines, cross hatch fill). (d) Ratio of $I = (a - b)/(a - c)$, showing whether the intermediate axis b is closer to a, making the body oblate-like, or closer to c, making the body prolate-like.

that have $a/b < 1.2$; few oblate-like bodies have $a/b > 1.5$ (Fig. 9c).

As mentioned above, virtually no bodies were perfectly oblate or prolate. The value I was computed for all primaries, which describes how near the body was to being exactly prolate or oblate (Fig. 9d). The plot shows that many bodies are very nearly completely prolate with b nearly equal to c. Conversely oblate-like primaries are frequently only mildly oblate, with b nearly evenly between a and c.

The observed population of NEA binaries typically have quite spherical primaries, where in most cases amplitude of the lightcurve is used to interpret the shape of the body. Some elongations could potentially be larger if the lightcurve amplitudes are artificially low due to non-ideal viewing angles. The simulations produce some low-elongation primaries, but relatively few in comparison with high-elongation bodies with elongation above 2.0. Furthermore, the simulated low-elongation primaries have a high probability of appearing oblate. When isolated, the low elongation primaries show no properties suggesting that they are more likely to have small separation or other properties related to the observed binary population. They have a slight trend toward lower eccentricity, possibly suggesting that the lack of observed high elongation primaries may be more related to survival, as opposed to formation. For example, how many of the currently observed binaries could survive with a primary of elongation 1.5 or 2.0? With all observed binaries having similarly small separations, studying orbital stability around irregularly shaped primaries is appropriate. An answer may be found in large-separation NEA binaries (when/if they are discov-

ered), where elongated primaries would have a less significant impact on the dynamics of the binary orbit, so the binaries may have a better chance of surviving long enough to be observed.

3.2. T-PROS and T-EEBs

Durda et al. (2004) introduced terminology to differentiate between two types of satellites formed in a collision. The SMAshed Target Satellites (SMATS) form from debris orbiting around a remaining target body. The Escaping Ejecta Binaries (EEBs) form from fragments escaping the collision and becoming bound to one another. Similar analogs exist in the case of a tidal disruption. We have dubbed systems that form around the largest remnant of the disruption "Tidal PROgenitor Satellites" (T-PROS), and those that form from escaping debris "Tidal Escaping Ejecta Binaries" (T-EEBs). As seen in the collisional cases, there are distinct differences between the two groups. The strongest difference is in size ratio, where the T-PROS have a high probability of having a size ratio between 0.1 and 0.2, while the T-EEBs have a strong chance of being 0.8 and higher (Fig. 10a). Some of this effect may be due to the resolution of the simulations, where if most of the 1000 particles are invested in the largest remnant, there are only limited remaining particles to create a T-EEB, which will then necessarily have size ratio near unity (to be considered, a clump must have at least 3 particles). This was also observed by Durda et al. (2004), where many of the EEBs are the lowest-resolution particles, thus having a size ratio of exactly 1. With only one NEA binary (Hermes) with a size ratio above 0.7, T-EEBs may not be common; in the simulations they made up only ∼10% of the total systems created, and have even stronger tendencies to come from extreme disruptions with low q and v_∞ (Figs. 10c and 10d).

There is also a distinct difference in the spin axis alignments for the two types (Fig. 10b). The T-PROS' primary spin axes are typically closely aligned with the binary orbital angular momentum, while the T-EEBs' primaries have only a slight correlation with the orbit. The T-PROS distribution matches that for the overall distribution, with close to 90% being aligned within 20° of the binaries' orbits. T-EEBs show only a slight alignment with the binary orbit, and has significant contributions out near 180°. The spin rates for the primaries of the T-EEBs are much more distributed than for T-PROS, and the secondaries have a similar distribution to that of all secondaries (not shown).

3.3. Classes of disruption

The three classes of disruption (S-, B-, and M-class; see Section 3.1) form binaries which have different properties. As well, each class of disruption prefers to form binaries from different types of encounters. First, the more disruptive the encounter, the more likely it was to have been produced by a low q or low v_∞ encounter. Figs. 11a and 11b show the relative contributions each of the three classes made as a function of q and v_∞. The resultant binaries from each class had some physical

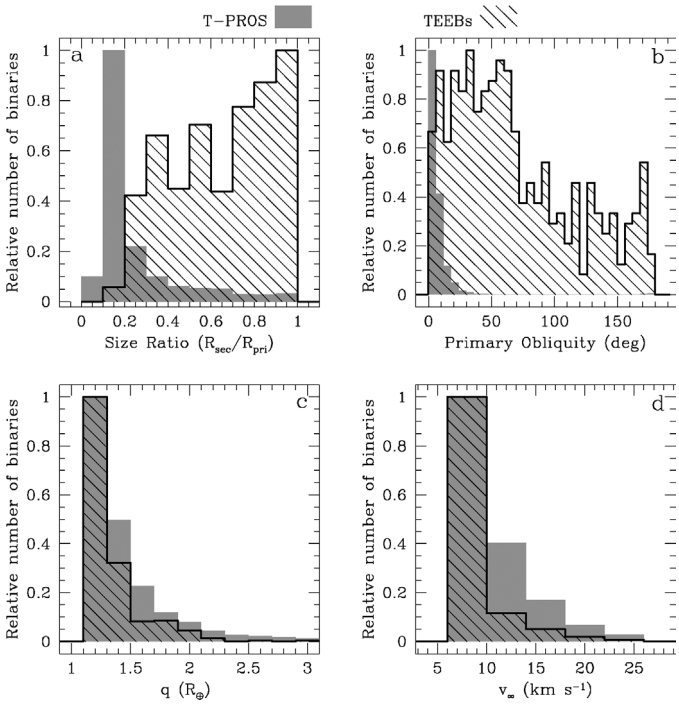

Fig. 10. Plots comparing T-PROS (shaded) with T-EEBs (bold lines) in terms of relative number, meaning each distribution is normalized independently due to large disparity in overall numbers: (a) secondary-to-primary size ratio; (b) primary obliquity; (c) relative binary formation as a function of encounter conditions q and (d) v_∞.

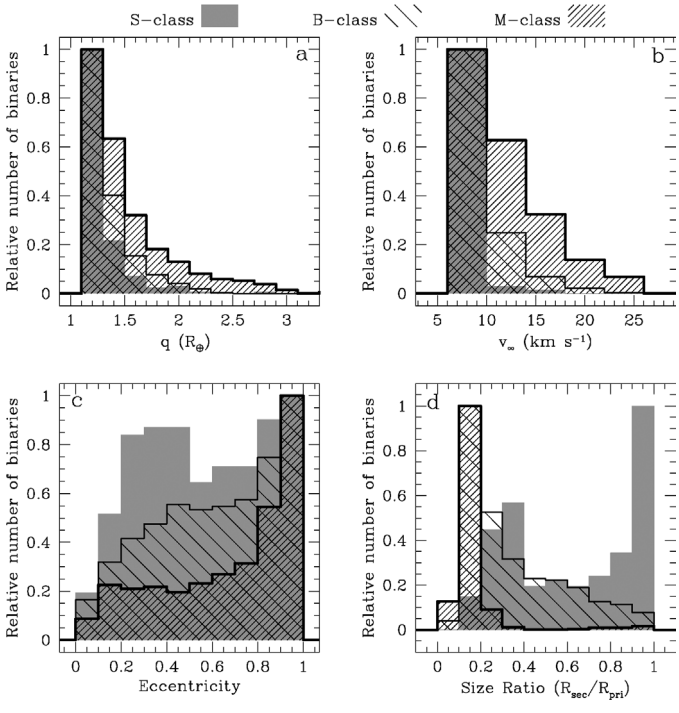

Fig. 11. Comparison of S-class (gray fill), B-class (wide cross-hatch) and M-class (small cross hatch) tidal disruptions in terms of relative number of binaries formed for each class. (a) The three classes are plotted as a function of close approach q and (b) v_∞. The binaries produced within each class are also plotted as a function of (c) eccentricity and (d) size ratio of the secondary to the primary.

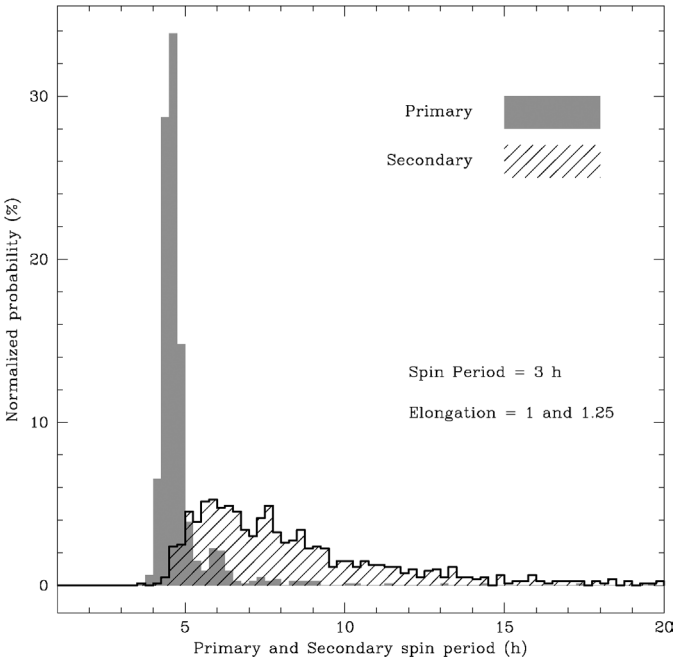

Fig. 12. Histograms of the primary (shaded) and secondary (cross-hatch) spin periods for the binaries produced in the 3-h spin subset.

differences, mostly in eccentricity and size ratio. Mild encounters had a stronger peak in high eccentricity, as compared to the S-class disruptions where a 0.95 eccentricity was only slightly more likely to occur than anything >0.25 (Fig. 11c). This trend continues in size ratio with mild encounters producing a strong peak between 0.1 and 0.2, while disruptive S-class encounters were peaked at 0.9–1.0 (Fig. 11d).

3.4. 3-h spin rate subset

The subset of simulations run with a progenitor 3-h spin period was done to investigate the relationship between the progenitor spin and the binary primary spin period. Of the 3-h simulations run, using only elongations of 1.0 and 1.25, 798 binaries were formed from 13,000 simulations. The 3-h subset produced a similar primary spin distribution to that of the entire set of simulations, with none below 3.7-h period (Fig. 12). Overall the periods for the primary and secondary were essentially the same for the full parameter simulation. This result suggests that primary spin is not strongly dependent on progenitor spin, and is likely dominated by other factors such as bulk density, particle shape or small internal strength.

3.5. Triples and hierarchical systems

In general, triple systems (a system with two secondaries orbiting one primary) are likely to be unstable on short timescales in the inner Solar System. Currently no asteroids have been observed in this state anywhere. However, the simulations produced these and more complicated systems with $N > 3$. The simplest case of two satellites orbiting the largest remnant was found in 757 of the simulations with another 357 having three or more satellites in orbit.

Some unique situations involved multiple systems formed around the second, third, and fourth largest remnant. There were 5 simulations with at least 2 secondaries around the second largest remnant, 6 that produced them around the third largest, and 1 simulation that produced them around the fourth largest remnant. These situations almost exclusively originated from very close encounters ($q < 1.6\ R_\oplus$) and fast-spinning primaries (4 h).

A hierarchical system, where a secondary has a bound companion, was a rare outcome. A total of 102 simulations produced these systems. These were typically simple situations with a satellite bound to the second-largest remnant, which in turn was bound to the largest remnant. Though no similar systems have been observed among asteroids, they do occur immediately post-disruption in simulations.

3.6. Tidal evolution and eccentricity damping

The simulations represent snapshots of binary properties immediately after formation. Subject to tidal interactions, planetary encounters, and thermal effects, the binaries will evolve with time. Tidal forces between the primary and secondary will affect the binary in most cases by: changing the semimajor axis of the secondary's orbit, synchronizing the secondary's rotation with its orbital period, and changing the eccentricity of the secondary. Weidenschilling et al. (1989) determined the change of the semimajor axis of a tidally evolving asteroid binary to be given by

$$\left(\frac{a_\mathrm{f}}{R_\mathrm{pri}}\right)^{13/2} - \left(\frac{a_0}{R_\mathrm{pri}}\right)^{13/2} = \frac{312\pi^{3/2}G^{3/2}\rho^{5/2}(R_\mathrm{sec}/R_\mathrm{pri})^3(1+(R_\mathrm{sec}/R_\mathrm{pri})^3)^{1/2}R_\mathrm{pri}^2}{19\sqrt{3}\mu Q} \times \Delta t, \tag{3}$$

where a_0 and a_f are the initial and final semimajor axes of the binary's orbit, G is the gravitational constant, ρ is the bulk density, μ is a measure of the rigidity of the body in dyn cm^{-2}, Q is the tidal dissipation factor, and Δt is time. The *effective* rigidity of a body, $\tilde{\mu}$, is defined as

$$\tilde{\mu} = \frac{19\mu}{2\rho g R}, \tag{4}$$

where $g = GM/R^2$ is the surface gravity of a body (Murray and Dermott, 1999).

Margot et al., 2002 obtained a value of $\tilde{\mu} = 1.66 \times 10^4$ for the radar-observed binary NEA 2000 DP_{107} by assuming the secondary had evolved from nearly touching the primary to its present separation over the median NEA lifetime of 10 Myr.[3]

For the known properties of 2000 DP_{107} ($D_\mathrm{pri} = 800$ m, $\rho = 1.7$ g cm^{-3}) and a commonly estimated value of $Q = 100$, the rigidity value is then $\mu = 2.26 \times 10^6$ dyn cm^{-2}. For comparison, solid rock has a value of μ near 10^{11} dyn cm^{-2} and

[3] The value constrained by Margot et al. (2002) was actually k_2/Q, where k_2 is the Love number and is related to rigidity by $k_2 = (3/2)/(1+\tilde{\mu})$.

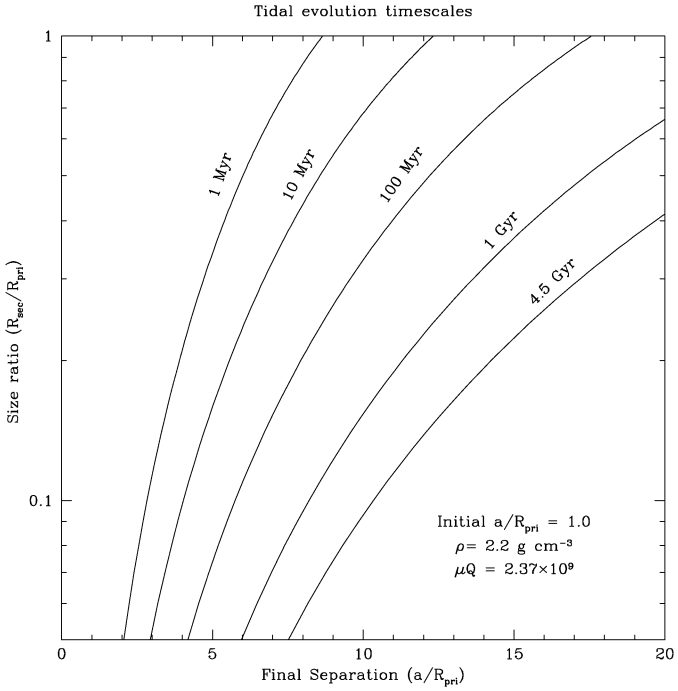

Fig. 13. The final separations ($a/R_{\rm pri}$) for different tidal evolution times for a binary starting at a separation of 1 $R_{\rm pri}$ as a function of their size ratio. The value for μQ used was 2.37×10^9 for a density of 2.2 g/cm^3.

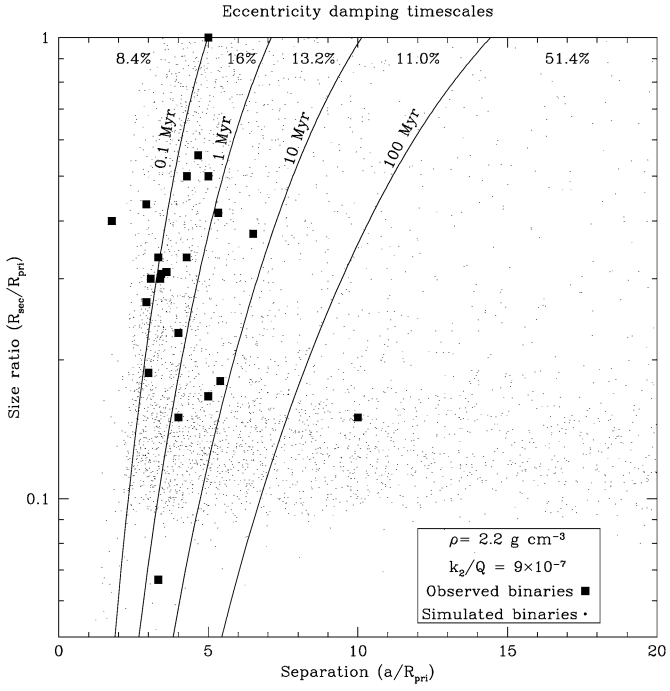

Fig. 14. The eccentricity damping timescales for binaries as a function of their size ratio and separation ($a/R_{\rm pri}$). Plotted as dots are the simulation-produced binaries and plotted as solid squares are the NEA binaries.

Phobos has μQ of 10^{12} dyn cm^{-2} (Weidenschilling et al., 1989; Yoder, 1981).

The values of $\mu Q = 2.26 \times 10^8$ dyn cm^{-2} and $\tilde{\mu} = 1.66 \times 10^4$ dyn cm^{-2} were used to estimate basic timescales for orbit evolution of the simulated binaries. $R_{\rm pri}$ was set at 1 km and the initial starting separation used for the calculations was 1.0 $R_{\rm pri}$; this simplification is made because the starting separation is largely insignificant for the relevant timescales (Fig. 13). The smaller size ratios evolve very slowly, with a binary of size ratio = 0.1 taking 10 Myr to evolve from a separation of 1 $R_{\rm pri}$ out to 4 $R_{\rm pri}$. Larger size ratios evolve much faster (as shown in Fig. 13), but have a smaller maximum attainable $a/R_{\rm pri}$ based on a simple conversion of initial primary spin to orbital angular momentum. For example, Hermes is presumed to be in a doubly synchronous state at <5 $R_{\rm pri}$ with a primary rotation and orbital period of $\sim$13.8 h (Pravec, 2003c; Margot et al., 2003). This binary represents a possible fully evolved system, with a small $a/R_{\rm pri}$ compared to a similar system with a smaller size ratio.

The calculations suggest that over a median NEA lifetime of 10 Myr the most observable effects of tidal evolution will be that binaries with near-equal-mass components approach a synchronous state quickly (Gladman et al., 2000). Orbital evolution is quite slow for smaller mass ratios, especially beyond 5 $R_{\rm pri}$.

Of the observed binary NEAs with known eccentricities, all but one have $e < 0.1$. The damping timescales of eccentricity due to tidal interactions is governed by

$$\tau_e = -\frac{e}{\dot{e}} = \frac{4}{63}\left(\frac{R_{\rm sec}}{R_{\rm pri}}\right)^3\left(\frac{a}{R_{\rm sec}}\right)^5\frac{\tilde{\mu}_{\rm sec}Q}{n}, \quad (5)$$

where n is the mean motion and $\tilde{\mu}_{\rm sec}$ is the effective rigidity of the secondary (Murray and Dermott, 1999). This formalism is for a secondary with a spin period equal to its orbital period and considers only the effects of the tides raised by the primary on the secondary. Tides raised on the primary by the secondary, which play a greater role for larger mass ratios, can have the effect of raising the secondary's eccentricity (Goldreich, 1963; Margot and Brown, 2003). Most of the known binaries have relatively small separations and size ratios, which is the regime in which eccentricity damping may be very efficient. Fig. 14 shows damping timescales as a function of size ratio and separation, with the simulated binaries and observed binaries indicated for reference. All but one observed binary has a damping timescale less than 10 Myr, and only 7 of the 24 have a damping timescale greater than 1 Myr. The outlier is 1998 ST_{27}, with a separation of 10 $R_{\rm pri}$ and an observed eccentricity >0.3. This is the only NEA binary with an eccentricity measured to be greater than 0.1, and is the only one for which the estimated damping timescale is greater than 10 Myr (Benner et al., 2003). This suggests that large-separation binaries discovered in the future may also have high eccentricities.

These evolution calculations are very dependent on $\tilde{\mu}_{\rm sec}$, for which the value used was derived from a single well-studied binary, 2000 DP_{107}. Not considered are other forces which may alter the binary on timescales comparable to those of mutual tidal forces, such as planetary tidal encounters or thermal effects. Previous work on binary encounters with Earth or Venus out to 8 planet radii showed that orbit properties of the binary can be altered dramatically (Chauvineau and Farinella, 1995; Bottke and Melosh, 1996a). In addition, the thermal

Yarkovsky and YORP effects have been identified as responsible for both orbital evolution and spin axis re-orientation of asteroids (Chesley et al, 2003; Vokrouhlický et al., 2003). Cuk and Burns (2004) propose that the YORP effect can alter the orbit of a synchronized secondary in a manner similar to how it affects a single body. Under ideal circumstances it may work on timescales as short as 10^5 yr, dominating tidal evolution in some situations.

4. Conclusions

This study used N-body simulations to model the tidal disruption of strengthless asteroids, or rubble piles, during close encounters with Earth. We presented distributions for the resultant physical and orbital properties of the binaries formed, citing similarities and differences with the observed population of NEA binaries. The spin of the primary body is bracketed in a similar fashion to the observed population, though the simulation's range of primary spin periods is centered on a somewhat slower spin period. Similarly, size ratios are smaller and less distributed than the observed binaries. Eccentricity poses one of the largest differences, with the simulations producing eccentricities greater than 0.1 for nearly all cases, whereas all observed binaries have eccentricity less than 0.1. Roughly half the simulated binaries had separations below 10 $R_{\rm pri}$, which is the upper limit for nearly all observed NEA binaries.

Due to the nature of the simulations, and the expensive computations involved, this many N-body runs cannot all be simulated forward to map the evolution of the overall population. Instead this task will have to be handled on a case-by-case basis, partly using analytical techniques developed by Scheeres (2002) to model evolution of binary systems with non-spherical primaries and secondaries. Other numerical techniques in development, such as freezing the rubble piles into rigid aggregates, thereby eliminating collision calculations, would reduce computation time making some stability and evolution simulations more practical.

As young binaries evolve and new binaries form, a steady-state distribution of properties may develop. Modeling this would help determine which binaries are created in the inner Solar System via tidal disruption and which, if any, may have entered intact from the Main Belt. Work by Chauvineau and Farinella (1995) and Bottke and Melosh (1996a) suggest further encounters of binaries with planets may increase the separation of binaries. Synthesis of these studies with this presented work could provide estimates of evolutionary tracks and help establish the steady-state distribution of properties.

An improvement in our knowledge of physical traits of small MBAs would help determine what effect tidal disruption has on the NEA population as a whole. Better determination of very small MBA shape and spin distributions will help set the initial conditions for future studies.

Overall this work points towards a population of NEA binaries yet to be discovered, those with small size ratio, and with separations greater than 10 $R_{\rm pri}$. This population could very well equal in numbers the current known small-separation binaries, and will likely be less uniform. These binaries may have elongated primaries, more eccentric orbits, and small size ratios.

Acknowledgments

The simulations were run on the `borg` and `vampire` computing clusters at the Department of Astronomy, University of Maryland. Thanks to Bill Bottke for providing encounter distributions and for manuscript comments. Thanks also to Doug Hamilton for manuscript comments. We thank the referees for helpful comments that improved the manuscript. This material is based upon work supported by the National Science Foundation under Grant No. AST0307549.

References

Asphaug, E., Benz, W., 1996. Size, density, and structure of Comet Shoemaker–Levy 9 inferred from the physics of tidal breakup. Icarus 121, 225–248.
Behrend, R., 2004. (4492) Debussy. IAU Circ. 8354.
Behrend, R., Bernasconi, L., Klotz, A., Durkee, R., 2004a. (854) Frostia. IAU Circ. 8389.
Behrend, R., Roy, R., Rinner, C., Antonini, P., Pravec, P., Harris, A.W., Sposetti, S., Durkee, R., Klotz, A., 2004b. (1089) Tama. IAU Circ. 8265.
Behrend, R., and 11 colleagues, 2004c. (1313) Berna. IAU Circ. 8292.
Belton, M., Carlson, R., 1994. 1993 (243). IAU Circ. 5948.
Benner, L.A.M., Nolan, M.C., Ostro, S.J., Giorgini, J.D., Margot, J.L., 2001a. 1998 ST_{27}. IAU Circ. 7730.
Benner, L.A.M., Ostro, S.J., Giorgini, J.D., Jurgens, R.F., Margot, J.L., Nolan, M.C., 2001b. 1999 KW_4. IAU Circ. 7632.
Benner, L.A.M., Nolan, M.C., Margot, J.L., Ostro, S.J., Giorgini, J.D., 2003. Radar imaging of binary near-Earth Asteroid 1998 ST_{27}. Bull. Am. Astron. Soc. 35, 959. Abstract.
Benner, L.A.M., Nolan, M.C., Ostro, S.J., Giorgini, J.D., Margot, J.L., Magri, C., 2004. 1999 DJ_4. IAU Circ. 8329.
Benz, W., Asphaug, E., 1999. Catastrophic disruptions revisited. Icarus 142, 5–20.
Bottke, W.F., Melosh, H.J., 1996a. Binary asteroids and the formation of doublet craters. Icarus 124, 372–391.
Bottke, W.F., Melosh, H.J., 1996b. The formation of asteroid satellites and doublet craters by planetary tidal forces. Nature 381, 51–53.
Bottke, W.F., Nolan, M.C., Greenberg, R., Kolvoord, R.A., 1994. Collisional lifetimes and impact statistics of near-Earth asteroids. In: Gehrels, T., Matthews, M.S. (Eds.), Hazards Due to Comets and Asteroids. Univ. of Arizona Press, Tucson, pp. 337–357.
Bottke, W.F., Richardson, D.C., Love, S.G., 1997. Note: Can tidal disruption of asteroids make crater chains on the Earth and Moon? Icarus 126, 470–474.
Bottke, W.F., Richardson, D.C., Michel, P., Love, S.G., 1999. 1620 Geographos and 433 Eros: Shaped by planetary tides? Astron. J. 117, 1921–1928.
Bottke, W.F., Morbidelli, A., Jedicke, R., Petit, J., Levison, H.F., Michel, P., Metcalfe, T.S., 2002. Debiased orbital and absolute magnitude distribution of the near-Earth objects. Icarus 156, 399–433.
Brown, M.E., Margot, J.L., Keck, W.M., de Pater, I., Roe, H., 2001. S/2001 (87) 1. IAU Circ. 7588.
Cellino, A., Pannunzio, R., Zappala, V., Farinella, P., Paolicchi, P., 1985. Do we observe light curves of binary asteroids? Astron. Astrophys. 144, 355–362.
Chauvineau, B., Farinella, P., 1995. The evolution of Earth-approaching binary asteroids: A Monte Carlo dynamical model. Icarus 115, 36–46.
Chesley, S.R., and 9 colleagues, 2003. Direct detection of the Yarkovsky effect by radar ranging to Asteroid 6489 Golevka. Science 302, 1739–1742.
Cuk, M., Burns, J.A., 2004. Effects of thermal radiation on the dynamics of binary NEAs. Bull. Am. Astron. Soc. 36, 1184. Abstract.
Donnison, J.R., Wiper, M.P., 1999. Bayesian statistical analysis of asteroid rotation rates. Mon. Not. R. Astron. Soc. 302, 75–80.

Durda, D.D., Bottke, W.F., Enke, B.L., Merline, W.J., Asphaug, E., Richardson, D.C., Leinhardt, Z.M., 2004. The formation of asteroid satellites in large impacts: Results from numerical simulations. Icarus 170, 243–257.

Gehrels, T., Drummond, J.D., Levenson, N.A., 1987. The absence of satellites of asteroids. Icarus 70, 257–263.

Gladman, B., Michel, P., Froeschlé, C., 2000. The near-Earth object population. Icarus 146, 176–189.

Goldreich, R., 1963. On the eccentricity of satellite orbits in the Solar System. Mon. Not. R. Astron. Soc. 126, 257–268.

Gradie, J., Flynn, L., 1988. A search for satellites and dust belts around asteroids: Negative results. Proc. Lunar Sci. Conf. XIX, 405–406. Abstract.

Guibout, V., Scheeres, D.J., 2003. Stability of surface motion on a rotating ellipsoid. Celest. Mech. Dynam. Astron. 87, 263–290.

Hamilton, D.P., Burns, J.A., 1991. Orbital stability zones about asteroids. Icarus 92, 118–131.

Harris, A.W., Young, J.W., Dockweiler, T., Gibson, J., Poutanen, M., Bowell, E., 1992. Asteroid lightcurve observations from 1981. Icarus 95, 115–147.

Holsapple, K.A., 2001. Equilibrium configurations of solid cohesionless bodies. Icarus 154, 432–448.

Leinhardt, Z.M., Richardson, D.C., 2002. *N*-Body simulations of planetesimal evolution: Effect of varying impactor mass ratio. Icarus 159, 306–313.

Leinhardt, Z.M., Richardson, D.C., 2005. A fast method for finding bound systems in numerical simulations: Results from the formation of asteroid binaries. Icarus 176, 432–439.

Leinhardt, Z.M., Richardson, D.C., Quinn, T., 2000. Direct *N*-body simulations of rubble pile collisions. Icarus 146, 133–151.

Magnusson, P., 1990. Spin vectors of 22 large asteroids. Icarus 85, 229–240.

Marchis, F., Descamps, P., Hestroffer, D., Berthier, J., Vachier, F., Boccaletti, A., de Pater, I., Gavel, D., 2003. A three-dimensional solution for the orbit of the asteroidal satellite of 22 Kalliope. Icarus 165, 112–120.

Marchis, F., Descamps, P., Hestroffer, D., Berthier, J., de Pater, I., 2004a. Fine analysis of 121 Hermione, 45 Eugenia, and 90 Antiope binary asteroid systems with AO observations. Bull. Am. Astron. Soc. 36, 1180. Abstract.

Marchis, F., Laver, C., Berthier, J., Descamps, P., Hestroffer, D., de Pater, I., Behrend, R., Roy, R., Baudoin, P., 2004b. (121) Hermione. IAU Circ. 8264.

Marchis, F., Berthier, J., Clergeon, C., Descamps, P., Hestroffer, D., 2005. On the diversity of binary asteroid orbits. In: Asteroids, Comets, and Meteors: ACM 2005. Abstract O10.1.

Margot, J.L., Brown, M.E., 2003. A low-density M-type asteroid in the main belt. Science 300, 1939–1942.

Margot, J.L., Keck, W.M., 2003. S/2003 (379) 1. IAU Circ. 8182.

Margot, J.-L., Brown, M.E., Keck, W.M., 2001. S/2001 (22) 1. IAU Circ. 7703.

Margot, J.L., Nolan, M.C., Benner, L.A.M., Ostro, S.J., Jurgens, R.F., Giorgini, J.D., Slade, M.A., Campbell, D.B., 2002. Binary asteroids in the near-Earth object population. Science 296, 1445–1448.

Margot, J.L., and 9 colleagues, 2003. 1937 UB (Hermes). IAU Circ. 8227.

Merline, W.J., and 10 colleagues, 1999a. Discovery of a moon orbiting the Asteroid 45 Eugenia. Nature 401, 565–568.

Merline, W.J., and 10 colleagues, 1999b. S/1998 (45) 1. IAU Circ. 7129.

Merline, W.J., Close, L.M., Dumas, C., Shelton, J.C., Menard, F., Chapman, C.R., Slater, D.C., 2000a. Discovery of companions to Asteroids 762 Pulcova and 90 Antiope by direct imaging. Bull. Am. Astron. Soc. 32, 1017. Abstract.

Merline, W.J., Close, L.M., Shelton, J.C., Dumas, C., Menard, F., Chapman, C.R., Slater, D.C., Keck, W.M., 2000b. Satellites of minor planets. IAU Circ. 7503.

Merline, W.J., Menard, F., Close, L., Dumas, C., Chapman, C.R., Slater, D.C., 2001. S/2001 (22) 1. IAU Circ. 7703.

Merline, W.J., Close, L.M., Siegler, N., Dumas, C., Chapman, C., Rigaut, F., Menard, F., Owen, W.M., Slater, D.C., 2002a. S/2002 (3749) 1. IAU Circ. 7827.

Merline, W.J., Tamblyn, P.M., Dumas, C., Close, L.M., Chapman, C.R., Menard, F., Owen, W.M., Slater, D.C., Pepin, J., 2002b. S/2002 (121) 1. IAU Circ. 7980.

Merline, W.J., Weidenschilling, S.J., Durda, D.D., Margot, J.L., Pravec, P., Storrs, A.D., 2002c. Asteroids do have satellites. In: Bottke Jr., W.F., Cellino, A., Paolicchi, P., Binzel, R.P. (Eds.), Asteroids III. Univ. of Arizona Press, Tucson, pp. 289–312.

Merline, W.J., Close, L.M., Dumas, C., Chapman, C.R., Menard, F., Tamblyn, P.M., Durda, D.D., 2003a. Discovery of new asteroid binaries (121) Hermione and (1509) Esclangona. Bull. Am. Astron. Soc. 35, 972. Abstract.

Merline, W.J., and 9 colleagues, 2003b. S/2003 (1509) 1. IAU Circ. 8075.

Merline, W.J., and 9 colleagues, 2003c. S/2003 (283) 1. IAU Circ. 8165.

Merline, W.J., Tamblyn, P.M., Chapman, C.R., Nesvorny, D., Durda, D.D., Dumas, C., Storrs, A.D., Close, L.M., Menard, F., 2003d. S/2003 (22899) 1. IAU Circ. 8232.

Merline, W.J., Tamblyn, P.M., Dumas, C., Close, L.M., Chapman, C.R., Menard, F., 2003e. S/2003 (130) 1. IAU Circ. 8183.

Merline, W.J., Tamblyn, P.M., Dumas, C., Menard, F., Close, L.M., Chapman, C.R., Duvert, G., Ageorges, N., 2004. S/2004 (4674) 1. IAU Circ. 8297.

Michel, P., Benz, W., Tanga, P., Richardson, D.C., 2001. Collisions and gravitational reaccumulation: Forming asteroid families and satellites. Science 294, 1696–1700.

Michel, P., Tanga, P., Benz, W., Richardson, D.C., 2002. Formation of asteroid families by catastrophic disruption: Simulations with fragmentation and gravitational reaccumulation. Icarus 160, 10–23.

Mottola, S., Lahulla, F., 2000. Mutual eclipse events in asteroidal binary system 1996 FG_3: Observations and a numerical model. Icarus 146, 556–567.

Mottola, S., Hahn, G., Pravec, P., Šarounová, L., 1997. S/1997 (3671). IAU Circ. 6680.

Murray, C.D., Dermott, S.F., 1999. Solar System dynamics. Cambridge Univ. Press, New York.

Neish, C.D., Nolan, M.C., Howell, E.S., Rivkin, A.S., 2003. Radar observations of binary Asteroid 5381 Sekhmet. In: American Astronomical Society Meeting Abstracts 203. Abstract #134.02.

Nolan, M.C., Margot, J.-L., Howell, E.S., Benner, L.A.M., Ostro, S.J., Jurgens, R.F., Giorgini, J.D., Campbell, D.B., 2000. 2000 UG_{11}. IAU Circ. 7518.

Nolan, M.C., Howell, E.S., Magri, C., Beeney, B., Campbell, D.B., Benner, L.A.M., Ostro, S.J., Giorgini, J.D., Margot, J.-L., 2002a. 2002 BM26. IAU Circ. 7824.

Nolan, M.C., Howell, E.S., Ostro, S.J., Benner, L.A.M., Giorgini, J.D., Margot, J.-L., Campbell, D.B., 2002b. 2002 KK_8. IAU Circ. 7921.

Nolan, M.C., Hine, A.A., Howell, E.S., Benner, L.A.M., Giorgini, J.D., 2003a. 2003 SS84. IAU Circ. 8220.

Nolan, M.C., Howell, E.S., Rivkin, A.S., Neish, C.D., 2003b. (5381) Sekhmet. IAU Circ. 8163.

Nolan, M.C., Howell, E.S., Hine, A.A., 2004. 2003 YT_1. IAU Circ. 8336.

Ostro, S.J., Hudson, R.S., Nolan, M.C., Margot, J., Scheeres, D.J., Campbell, D.B., Magri, C., Giorgini, J.D., Yeomans, D.K., 2000a. Radar observations of Asteroid 216 Kleopatra. Science 288, 836–839.

Ostro, S.J., Margot, J.-L., Nolan, M.C., Benner, L.A.M., Jurgens, R.F., Giorgini, J.D., 2000b. 2000 DP_{107}. IAU Circ. 7496.

Ostro, S.J., Hudson, R.S., Benner, L.A.M., Giorgini, J.D., Magri, C., Margot, J.L., Nolan, M.C., 2002. Asteroid radar astronomy. In: Bottke Jr., W.F., Cellino, A., Paolicchi, P., Binzel, R.P. (Eds.), Asteroids III. Univ. of Arizona Press, Tucson, pp. 151–168.

Ostro, S.J., Nolan, M.C., Benner, L.A.M., Giorgini, J.D., Margot, J.L., Magri, C., 2003. 1990 OS. IAU Circ. 8237.

Pravec, P., Hahn, G., 1997. Two-period lightcurve of 1994 AW_1: Indication of a binary asteroid. Icarus 127, 431–440.

Pravec, P., Harris, A.W., 2000. Fast and slow rotation of asteroids. Icarus 148, 12–20.

Pravec, P., Wolf, M., Šarounová, L., 1998. Lightcurves of 26 near-Earth asteroids. Icarus 136, 124–153.

Pravec, P., Wolf, M., Šarounová, L., 1999. How many binaries are there among the near-Earth asteroids? In: IAU Colloq. 173: Evolution and Source Regions of Asteroids and Comets, p. 159.

Pravec, P., Kušnirá, P., Hicks, M., Holliday, B., Warner, B., 2000a. 2000 DP_{107}. IAU Circ. 7504.

Pravec, P., and 10 colleagues, 2000b. Two-period lightcurves of 1996 FG_3, 1998 PG, and (5407) 1992 AX: One probable and two possible binary asteroids. Icarus 146, 190–203.

Pravec, P., Kušnirá, P., Warner, B., 2001. 2001 SL_9. IAU Circ. 7742.

Pravec, P., Harris, A.W., Michalowski, T., 2002. Asteroid rotations. In: Bottke Jr., W.F., Cellino, A., Paolicchi, P., Binzel, R.P. (Eds.), Asteroids III. Univ. of Arizona Press, Tucson, pp. 113–122.

Pravec, P., and 11 colleagues, 2003a. (65803) 1996 GT. IAU Circ. 8244.
Pravec, P., and 10 colleagues, 2003b. (66063) 1998 RO_1. IAU Circ. 8216.
Pravec, P., and 15 colleagues, 2003c. 1937 UB (Hermes). IAU Circ. 8233.
Pravec, P., Kušnirák, P., Šarounová, L., Brown, P., Kaiser, N., Masi, G., Mallia, F., 2004a. 1999 DJ_4. IAU Circ. 8316.
Pravec, P., and 36 colleagues, 2004b. Photometric survey of binary near-Earth asteroids. Bull. Am. Astron. Soc. 36, 1131. Abstract.
Pravec, P., and 53 colleagues, 2005. Photometric survey of binary near-Earth asteroids. Icarus. In press.
Reddy, V., Dyvig, R., Pravec, P., Kušnirák, P., 2005. 2005 AB. IAU Circ. 8483.
Richardson, D.C., Bottke, W.F., Love, S.G., 1998. Tidal distortion and disruption of Earth-crossing asteroids. Icarus 134, 47–76.
Richardson, D.C., Quinn, T., Stadel, J., Lake, G., 2000. Direct large-scale *N*-body simulations of planetesimal dynamics. Icarus 143, 45–59.
Richardson, D.C., Leinhardt, Z.M., Melosh, H.J., Bottke, W.F., Asphaug, E., 2002. Gravitational aggregates: Evidence and evolution. In: Bottke Jr., W.F., Cellino, A., Paolicchi, P., Binzel, R.P. (Eds.), Asteroids III. Univ. of Arizona Press, Tucson, pp. 501–515.
Richardson, D.C., Elankumaran, P., Sanderson, R.E., 2005. Numerical experiments with rubble piles: Equilibrium shapes and spins. Icarus 173, 349–361.
Roberts, L.C., McAlister, H.A., Hartkopf, W.I., Franz, O.G., 1995. A speckle interferometric survey for asteroid duplicity. Astron. J. 110, 2463–2468.
Ryan, W.H., Ryan, E.V., Martinez, C.T., Stewart, L., 2003. (3782) Celle. IAU Circ. 8128.
Ryan, W.H., Ryan, E.V., Martinez, C.T., 2004. 3782 Celle: Discovery of a binary system within the Vesta family of asteroids. Planet. Space Sci. 52, 1093–1101.
Scheeres, D.J., 2002. Stability of binary asteroids. Icarus 159, 271–283.
Scheeres, D.J., Ostro, S.J., Werner, R.A., Asphaug, E., Hudson, R.S., 2000. Effects of gravitational interactions on asteroid spin states. Icarus 147, 106–118.
Scheeres, D.J., Marzari, F., Rossi, A., 2004. Evolution of NEO rotation rates due to close encounters with Earth and Venus. Icarus 170, 312–323.
Schenk, P.M., Asphaug, E., McKinnon, W.B., Melosh, H.J., Weissman, P.R., 1996. Cometary nuclei and tidal disruption: The geologic record of crater chains on Callisto and Ganymede. Icarus 121, 249–274.
Shepard, M.K., Schlieder, J., Nolan, M.C., Hine, A.A., Benner, L.A.M., Ostro, S.J., Giorgini, J.D., 2004. 2002 CE_26. IAU Circ. 8397.
Solem, J.C., 1994. Density and size of Comet Shoemaker–Levy 9 deduced from a tidal breakup model. Nature 370, 349–351.
Solem, J.C., Hills, J.G., 1996. Shaping of Earth-crossing asteroids by tidal forces. Astron. J. 111, 1382–1387.
Stadel, J.G., 2001. Cosmological *N*-body simulations and their analysis. Ph.D. thesis, p. 126.
Stanzel, R., 1978. Lightcurves and rotation period of minor planet 283 Emma. Astron. Astrophys. Suppl. 34, 373–376.
Storrs, A., Weiss, B., Zellner, B., Burleson, W., Sichitiu, R., Wells, E., Kowal, C., Tholen, D., 1999. Imaging observations of asteroids with Hubble Space Telescope. Icarus 137, 260–268.
Storrs, A., Vilas, F., Landis, R., Wells, E., Woods, C., Zellner, B., Gaffney, M., 2001. S/2001 (107) 1. IAU Circ. 7599.
Tamblyn, P.M., Merline, W.J., Chapman, C.R., Nesvorny, D., Durda, D.D., Dumas, C., Storrs, A.D., Close, L.M., Menard, F., 2004. S/2004 (17246) 1. IAU Circ. 8293.
Tanga, P., Hestroffer, D., Berthier, J., Cellino, A., Lattanzi, M.G., di Martino, M., Zappalá, V., 2001. Note: HST/FGS observations of the Asteroid (216) Kleopatra. Icarus 153, 451–454.
van Flandern, T.C., Tedesco, E.F., Binzel, R.P., 1979. Satellites of asteroids. In: Gehrels, T. (Ed.), Asteroids. Univ. of Arizona Press, Tucson, pp. 443–465.
Vokrouhlický, D., Nesvorný, D., Bottke, W.F., 2003. The vector alignments of asteroid spins by thermal torques. Nature 425, 147–151.
Walsh, K.J., Richardson, D.C., Rettig, T.W., 2003. Modeling the breakup of Comet Shoemaker–Levy 9. In: Hubble's Science Legacy: Future Optical/Ultraviolet Astronomy from Space, ASP Conf. Ser. 291, pp. 415–418.
Warner, B.D., 2004. The minor planet observer. http://www.minorplanetobserver.com/htms/pdo_lightcurves.htm.
Warner, B., Pravec, P., Harris, A.W., Galád, A., Kušnirák, P., 2005a. Binary Hungarias (5905) Johnson and (9069) Hovland: Their relations to small binary Vestoids and NEAs. In: Asteroids, Comets, and Meteors: ACM 2005. Abstract P10.14.
Warner, B., Pravec, P., Kušnirák, P., Pray, D., Galád, A., Gajdoš, S., Brown, P., Krzeminski, Z., 2005b. (5905) Johnson. IAU Circ. 8511.
Weidenschilling, S.J., Paolicchi, P., Zappala, V., 1989. Do asteroids have satellites? In: Binzel, P., Gehrels, T., Matthews, M.S. (Eds.), Asteroids II. Univ. of Arizona Press, Tucson, pp. 643–658.
Yoder, C.F., 1981. Effect of resonance passage on the tidal evolution of Phobos' orbit. Bull. Am. Astron. Soc. 13, 710. Abstract.